Economy of Tokamak Neutron Source for Transmutation of Transuranics

Ryosuke SAKAI, Takaaki FUJITA and Atsushi OKAMOTO
Nagoya University, Furo-cho, Chikusa-ku, Nagoya 464-8603, Japan
(Received 18 March 2018 / Accepted 11 November 2018)

This paper evaluates the economy of a tokamak neutron source for transuranics transmutation using the Physics-Engineering-Cost system code. We compared two devices, one with normal conductive coil (NCC) and another with superconducting coil (SCC). The plasma performance was assumed to be moderate ones. The cost of neutron (CON) was used to measure the economy, taking into account the selling net electricity ($P_{\mathrm{e-net}}$). We scanned the plasma aspect ratio (A) and thickness of inboard-side shield of an NCC device. It was revealed that ohmic loss in the magnetic coils (P_{coil}) is the dominant factor on determining the optimum aspect ratio for the economy of an NCC device. On the other hand, in an SCC device, the dependence of CON on the aspect ratio is relatively weak due to the absence of P_{coil} and smaller weight of the coils. Moreover, as the inboard-side shield of an NCC device became thicker, the economy of the device became worse. It was found that enough plant availability in SCC settings, which presupposes development of a remote-handling system, results in the relatively higher economic potential of SCC settings than of NCC settings.

Keywords: neutron source, transuranic, aspect ratio, normal conductive coil, superconducting coil, circulating power, cost

DOI: 10.1585/pfr.14.1405040

1. Introduction

Long-lived transuranic (TRU) wastes produced by nuclear fission power plants are known as radioactive and biohazard materials. At present, these biohazardous nuclear wastes are being buried deep under the ground (deep geological disposal); however, lands, where these wastes of a million-year half-life can be contained safely, are limited.

Transmutation as another method of disposal has attracted the attention of research enthusiasts. In this process, the long-lived nuclei are converted into nuclei with shorter half-life by fast neutrons, during fission or neutron capture reaction. The current schemes of nuclear waste transmutation include the accelerator-driven subcritical reactor (ADS), fission reactor (FR), and fast breeder reactor (FBR). ADS has no risks of serious accidents such as meltdown; however, it has relatively low fast neutron flux and large device size. In contrast, FR and the FBR have relatively high neutron flux and smaller sizes, and exhibit higher risks of serious accidents; furthermore, they consume fast neutrons for themselves to maintain chain reactions, leading to low transmutation efficiency.

In contrast, fusion reactors can irradiate high flux fast neutrons by deuterium and tritium fusion reaction. Fusion reactors have relatively low risks because of their difficulty in maintaining fusion reaction and have a size relatively smaller than the ADS [1]. These reactors have the potential to supply plenty of fast neutrons for transmutation, at low costs.

M. Kotcheunreuther et al. [2] proposed the fusion–fission transmutation system by compact fusion neutron source (CFNS) with normal conductive coil (NCC), a system based on a fusion–fission hybrid reactor where fast neutrons strongly augment the rate of nuclear reactions in a surrounding subcritical fission blanket fueled by transuranics. On the other hand, W.M. Stacey et al. [3] proposed the Subcritical Advanced Burner Reactor (SABR), a tokamak-type fusion reactor with superconducting coil (SCC). Plasma configuration such as plasma aspect ratio A is fixed in both CFNS and SABR.

The economics of tokamak fusion neutron source for transmutation of TRU has been rarely studied. We studied the A dependence of the cost of the neutron source with NCC and found that the minimum cost per neutron is approximately $A \sim 2.2$ [4]. The optimum A is mainly determined by the electric power of field coils, and though it depends on the thickness of the inboard-side shield, it was not scanned in [4].

In this study, we have scanned the thickness of the inboard-side shield of NCC settings and compared the neutron sources with NCC and SCC. The NCC consumes electric power (ohmic loss). However, since the NCCs can be disassembled if they have a small number of turns, maintenance and replacement of in-vessel components are relatively easy. Tokamak designs with demountable NCCs offer a very attractive option for the device in which rapid replacement is essential [5]. However, the

author's e-mail: sakai-ryosuke15@ees.nagoya-u.ac.jp

lifetime of the Center Post (CP) can be a dominant factor for plant availability of NCC devices. In the ARIES–ST, which has NCC, the lifetime of CP was estimated three years for an average neutron wall load of 4.10 MWm^{-2} and inboard shield thickness (t_{sh}) of approximately 0.26 m [6, 7]. In this study, the average neutron wall load is only ~0.60 MWm^{-2}, the t_{sh} of NCC is 0.26 m for the standard value, and the burn cycle of SABR is 750 days [3], which is less than three years. Thus, the CP lifetime will be sufficiently longer than the burn cycle of "Fission Fuel Region" (FFR) discussed here, and then the duration of continuous operation will be determined by replacement of the blanket modules, divertor assemblies, and shields, in both NCC devices and SCC devices. In SCC devices, the development of a complicated remote-handling system for maintenance and replacement of in-vessel components is imperative, since the SCCs cannot be disassembled. The work will be more difficult and time-consuming, even with the remote-handling system, than in NCC devices because the SCC devices tend to be larger as will be shown in the subsequent sections. Furthermore, the duration for cooling down the SCCs, which is typically one month, is also necessary before tokamak operation after maintenance, though warming up the SCCs before maintenance might be done while waiting for the reduction of decay heat in activated components. From these two reasons, the maintenance period between operations will be shorter, and hence, higher availability is expected in NCC devices than in SCC devices. On the other hand, because there is no ohmic loss in SCCs, their electric power consumption will be smaller than in NCC devices. The tradeoff between availability and electric power consumption in NCC and SCC devices is one of the subjects of this paper.

The design parameters and the cost were evaluated by the PEC (Physics-Engineering-Cost) system code [8].

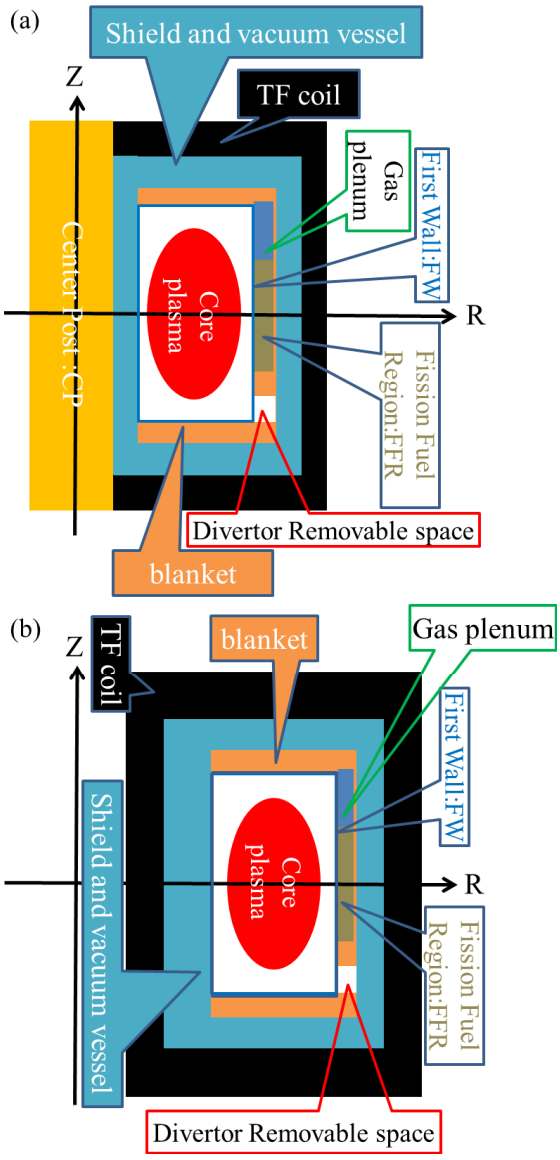

Fig. 1 Geometric configurations of (a) an NCC device and (b) an SCC device. In case of NCC settings, the CP has the largest possible radius to minimize its ohmic loss. In case of SCC settings, the cross-sectional area of the TF coils is determined by fixed current density limit (20.3 MAm^{-2} [10]), and the required coil current. The structure of the blanket including the fission core is basically the same as that in SABR [3].

2. Models and Conditions for Analysis

2.1 Geometric configuration and coil model

The schematic device in this study and its radial build are shown in Figs. 1 and 2, respectively. The structure of the blanket, including the FFR, is basically the same as assumed in SABR [3], which is described in detail in the next subsection. In an NCC device, as shown in Figs. 1 (a) and 2 (a), the CP and the outer toroidal field coils connected to it generate the toroidal fields. It is assumed that the connection between the CP and the coils can be disassembled for maintenance, like the CTF concept [9]. The CP is assumed to fill the whole available space in the central region inside the shield or the vacuum vessel to minimize the ohmic loss. The radius of CP, R_{CP}, is determined by:

$$R_{CP} = (1 - 1/A)R_P - \Delta_{in} - t_{sh}, \quad (1)$$

where R_P is the plasma major radius, Δ_{in} is the gap between the plasma surface and the inner first wall (FW), and t_{sh} is the thickness of the inner shield and the FW. We did not consider the limit of current density and the magnetic field strength inside the CP, and hence, we have no lower limit, by electromagnetic condition, of A in an NCC device.

In contrast, in an SCC device, as shown in Figs. 1 (b) and 2 (b), conventional TF coils are assumed. The cross-sectional area of the TF coils, S_{TF}, is determined by the fixed current density limit (20.3 MAm^{-2} [10]) and the required coil current, I_{coil}, which is given by $I_{coil} = 2\pi R_P B_T/\mu_0$ from Ampere's law, where B_T is the toroidal field at the plasma center, and μ_0 is the permeability of vacuum. (See Fig. 2 (b) for geometric understanding). The

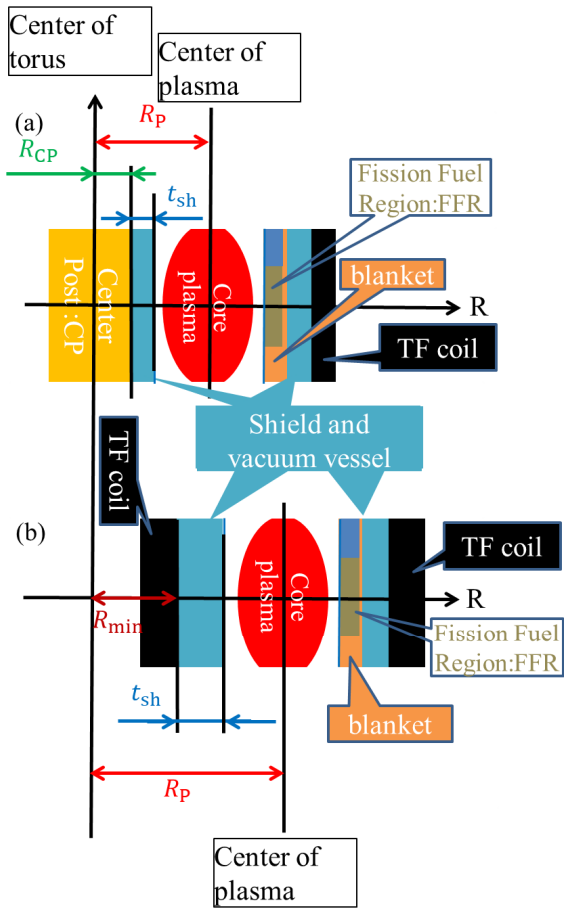

Fig. 2 Radial build of the device of (a) NCC settings and (b) SCC settings. R_P is the plasma major radius. R_{CP} is the radius of CP. R_{min} is the distance from the center of torus to the inner (plasma side) surface of inboard TF coils at the equatorial plane. t_{sh} is the thickness of the inboard shield.

TF thickness of SCC, t_{TF}, is determined by

$$t_{TF} = R_{min} - \sqrt{R_{min}^2 - S_{TF}/\pi}, \quad (2)$$

where R_{min} is the distance from the center of torus to the inner (plasma side) surface of inboard TF coils at the equatorial plane. R_{min} is determined by the right side of Eq. (1).

Therefore, as shown in Fig. 1, we have a space in the central region of the device inside the inboard TF coils of the SCC devices so that in general, they are thinner than those in NCC. We assumed that the critical magnetic field of SCC is 11.8 T [10]. The lower limit of A in an SCC device is determined by the condition that the whole central space is used for the inboard TF coils, or that the maximum field reaches the critical value. The ohmic coil for the inductive current drive is not equipped. We assumed that the plasma current is ramped up by a neutral beam current drive. The poloidal field coils are counted for cost and electricity consumption (ohmic loss) in an NCC device, and for the cost in an SCC device, though their positions have not been decided. We also fixed the t_{sh} to 0.675 m in an SCC device, which corresponds to the thickness of the inboard shield of SABR [3]. In an NCC device, the standard value of t_{sh} is 0.26 m, which corresponds to that in the ARIES–ST design [7] and the same as used in [4], is scanned around it.

2.2 Blanket models

In the SABR blanket design, the thermal power output was fixed to 3 GW and the fusion power was increased from 100 to 180 MW during the fuel cycle [3]. The TRU fuel, composed of 40%Zr–10%Am–10%Np–40%Pu, was contained in the FFR on the outboard-side [3]. The tritium breeding was planned in the upper and lower blankets, and in the outer blanket of FFR that contains Li_2SiO_4 [3]. We did not calculate the neutron transport or nuclear reactions but referred to the SABR blanket design. In our previous study [4], it was assumed that the same performance on transmutation of TRUs and the same fission power would be achieved with the same outer FW area and the same fusion power. However, the fusion neutrons that directly enter the FFR mainly determine the performance on the transmutation of TRUs and the fission power. Thus, in our previous study [4], the same area of the outer first wall did not necessarily result in the same FFR area, because we have an area for other purposes including the divertor removal space. We have also assumed a D-shape blanket while the fission-core is cylindrical [4]. Therefore, in this study, we assumed a cylindrical design such as the SABR [3], as shown in Figs. 1 and 2, and fixed the FW surface area in front of FFR, the volume of FFR, and the fusion neutron power applied for the FW surface in front of FFR to those used in SABR [3]. Namely, we fixed the FW surface area in front of FFR, S_{FFR} to 62.4 m^2 and the volume of FFR to 41.4 m^3, fixed by the thickness of the outboard blanket, where the area and the volume for the gas plenum are excluded. This value of S_{FFR} determines the device size, including plasma major radius for each A, under the assumptions stated below. The ratio of the length of FFR to the total length of the fission core (fuel pin) and also to the height of the outer (and inner) FW, are fixed to those used in SABR. The former implies that the height of the gas plenum should be half that of FFR as in SABR [3]. The latter is achieved by assuming that the ratio of the height of components contained in the outer blanket, other than the fission core, namely, structural material, TBR blanket, and reflector, to the total height of the FW is the same as that in SABR. The thickness of the outer blanket is almost the same as that in SABR. The elevation views of the tokamak with Fission Core for an NCC device with $A = 1.625$ and for an SCC device with $A = 3.5$ are shown in Fig. 3.

The fusion power required is determined assuming that fusion neutrons are uniformly distributed on the total FW area. Namely, in PEC, the fusion power P_{fus} is determined so that $P_{fus}S_{FFR}/S_{FW} = P_{fus}^{SABR}S_{FFR}^{SABR}/S_{FW}^{SABR} = 39.1$ MW. Here S_{FW} is the total first wall area in PEC, and S_{FW}^{SABR}, the total FW area in SABR, is 289 m^2. Conse-

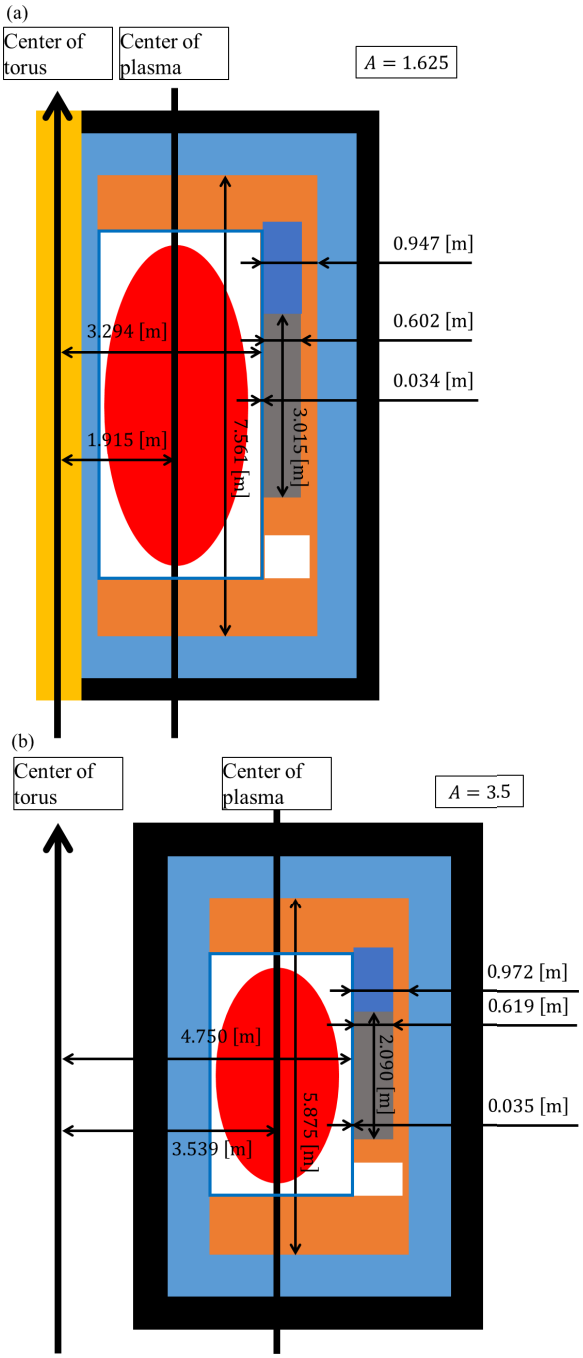

Fig. 3 Elevation views of the tokamak with Fission Core for both (a) minimum A for NCC and (b) maximum A for SCC. The total thickness of the outer blanket and the thickness of FW are 0.947 m and 0.972 m, respectively. The thickness of FFR, which does not include the thickness of FW, are 0.602 m and 0.619 m. The thickness of the FW are 0.034 m and 0.035 m.

quently, $P_{\rm fus}S_{\rm FFR}/S_{\rm FW} = P_{\rm fus}^{\rm SABR}S_{\rm FFR}^{\rm SABR}/S_{\rm FW}^{\rm SABR} = 180\,[\rm MW]\cdot 62.4\,[\rm m^2]/289\,[\rm m^2] = 39.1\,[\rm MW]$ [3]. The $P_{\rm fus}^{\rm SABR}$ is fixed to the maximum value of 180 MW during the fuel cycle planned in SABR for simplicity [3,4]. These are target values in this study. We assumed that the subcriticality of the devices is the same as SABR for all A because the thickness of FFR is almost the same as SABR.

2.3 Plasma models

The plasma aspect ratio A dependence of plasma elongation κ [11], and the dependence on A and κ of the normalized plasma beta $\beta_{\rm N}$ [12], are assumed as

$$\kappa = \frac{1.1996}{A^2} + \frac{0.4041}{A} + 1.5322, \tag{3}$$

$$\beta_{\rm N} = \frac{1}{f_{\rm peak}^{0.5}}\left(3.09 + \frac{3.35}{A} + \frac{3.87}{A^{0.5}}\right)\left(\frac{\kappa}{3}\right)^{0.5}, \tag{4}$$

where $f_{\rm peak}$ denotes the peaking factor of the plasma pressure. The formula for κ used in this study, Eq. (3), is different with that in our previous study [4] that was based on [12]. The present formula has lower κ in $1.0 < A < \sim 4.5$. The formula for $\beta_{\rm N}$ is fitted by a simpler function of A for simplicity [4],

$$\beta_{\rm N} = \beta_{\rm N0}\left(\frac{3}{A}\right)^{0.39}\left(\frac{\kappa}{2}\right)^{0.5}, \tag{5}$$

where $\beta_{\rm N0}$ is an input parameter and fixed at 3 in this study. The density n and temperature T profiles in plasma are shown as below,

$$n(\rho) = n_0(1-\rho^2)^{a_{\rm n}}, \tag{6}$$

$$T(\rho) = T_0(1-\rho^2)^{a_{\rm t}}, \tag{7}$$

where ρ is the normalized minor radius. In this study, we fixed $a_{\rm n}$ and $a_{\rm t}$ to 0.25 and 1.0, respectively, and assumed $T_0 = 15\,\rm keV$. The density is determined by $\beta_{\rm N}$ and the magnetic field of toroidal coil, $B_{\rm max}$. We also assumed that $q^* \geq 2.5$ and $q_{95} \geq 3$, considering the operation regimes of ST ($q^* \geq 2.5$) [13] and of the conventional tokamak ($q_{95} \geq 3$). The relation of q^* and q_{95} is shown as

$$\frac{q_{95}}{q^*} = \frac{1.17 - 0.65A^{-1}}{(1-A^{-2})^2}. \tag{8}$$

The ratio q_{95}/q^* is 1.2 at $A = 3.0$, and decreases with A. Hence, the lower limit of the safety factor is determined by $q^* \geq 2.5$ in $A \leq 3.0$, and by $q_{95} \geq 3$ in $A \geq 3.0$.

Figure 4 shows the dependence of κ, $\beta_{\rm N}$, q^*, q_{95}, and $R_{\rm P}$ on A for the fixed $S_{\rm FFR}$.

We assumed deuterium neutral beam (NB) injection for heating and current drive (CD), with the beam energy at 200 keV for quasi-perpendicular injection for heating, and at 800 keV for co-tangential injection for CD. The beam-thermal fusion power is considered in this study. We fixed the CD efficiency and the gain for beam-thermal fusion to $\eta_{\rm CD} = 0.2\times10^{20}\,\rm AW^{-1}m^{-2}$, $Q_{\rm b-th} = 0.25$ for CD NB, and $Q_{\rm b-th} = 0.5$ for heating NB.

We took standard ITER H-mode scaling [9] for energy confinement times $\tau_{\rm E}$. The formula here is

$$\tau_{\rm E} = H_{98y2}\frac{0.0562M^{0.19}I_{\rm P}^{0.93}R_{\rm P}^{1.97}B_{\rm T}^{0.15}\kappa^{0.78}\bar{n}_{19}^{0.41}}{A^{0.58}(f_{\rm alpconf}P_\alpha + P_{\rm aux} + P_{\rm CD})^{0.69}}, \tag{9}$$

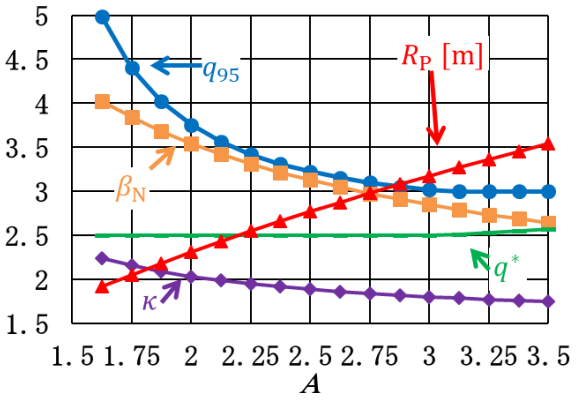

Fig. 4 Dependence of κ, β_N, q^*, q_{95}, and R_P on A.

where H_{98y2}, M, I_P, B_T, and $\bar{n}_{19}$ represents the enhancement factor (in this study, $H_{98y2} = 1.0$), the average plasma ion mass number (because we took deuterium and tritium fusion reaction, $M = 2.5$), the plasma currents in MA, the toroidal field at the plasma center in T, and the line average electron density in 10^{19} m^{-3}, respectively. The expression $f_{alpconf}P_\alpha + P_{aux} + P_{CD}$ corresponds to the input power for fusion plasma, and $f_{alpconf}$, P_α, P_{aux}, and P_{CD} denote confinement factor of α particles (assumed to be 98%), α particle heating power in MW, quasi-perpendicular NB power in MW, and co-tangential injection NB power in MW, respectively.

The calculation flow chart of PEC code used herein is shown in Fig. 5. First, R_P is determined so that FFR surface area, $S_{FFR} = 62.4\,\text{m}^2$, at each input A. Then, B_{max} is adjusted to regulate the toroidal field B_T to suffice $P_{fus}(S_{FFR}/S_{FW}) = 39.1\,\text{MW}$. The procedure to calculate P_{fus} with B_T is as follows. We assumed that the safety factor is the lowest value ($q^* = 2.5$ in $A \le 3.0$ or $q_{95} = 3$ in $A \ge 3.0$), and that the plasma current I_P is determined by B_T. As β_N is determined by A in Eq. (5), the plasma pressure is obtained. The density profile is then determined because the temperature profile is fixed. These two profiles are then used to calculate thermal fusion power. The total NB power and CD NB power are determined by energy confinement time given by Eq. (9) and by the given CD efficiency, respectively. If the CD NB power exceeds the total NB power, we increased the safety factor. The beam-thermal fusion power is calculated with obtained NB powers and the given Q_{b-th}. Finally, P_{fus} is obtained by summing thermal and beam-thermal fusion power.

2.4 Power balance

Figure 6 illustrates the energy flow of fusion neutron source. The thermal power generated in the blanket comes from the power produced in the FFR by fission of TRUs. We fixed the thermal power P_{th} to 3 GW (thermal) and the gross electricity $P_{e-gross}$ to 1049 MW (electric) in reference to the SABR design [3]. $P_{e-recirc}$, P_{e-net}, and P_{coil} represent the circulating power, the net electricity, and the power

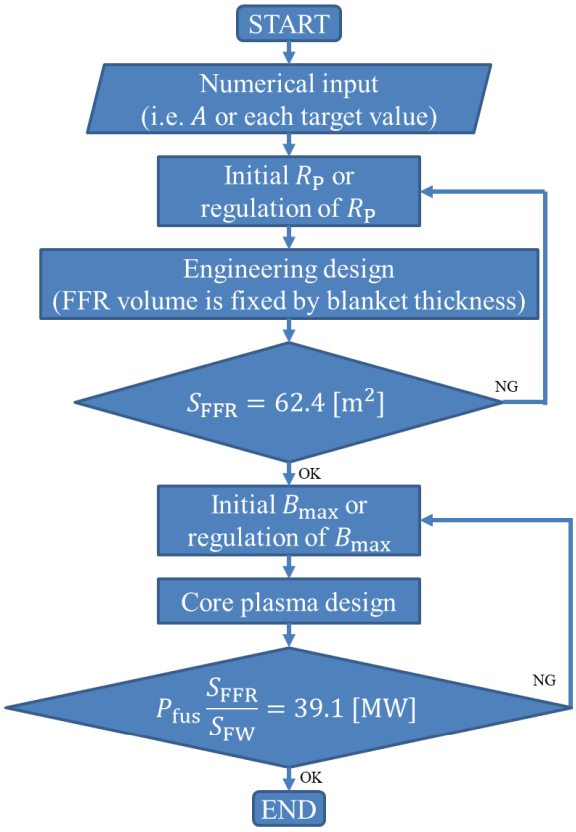

Fig. 5 The calculation flow chart of PEC code in this study. S_{FFR}, B_{max}, P_{fus}, and S_{FW} are the FW surface area in front of FFR, the magnetic field of toroidal coil, the plasma fusion power, and the total first wall area, respectively.

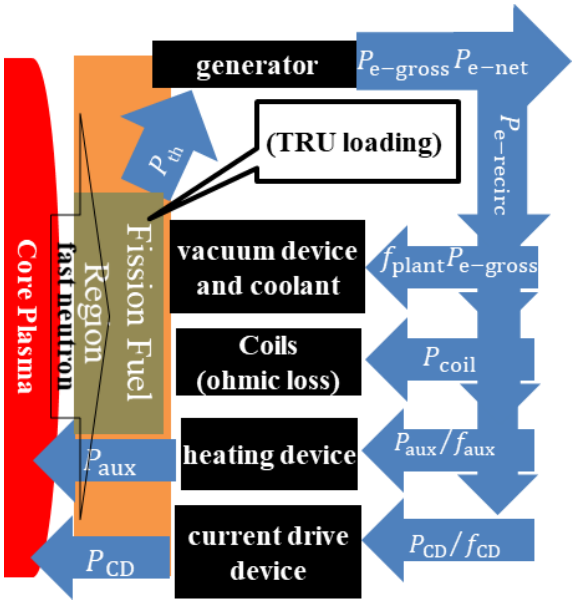

Fig. 6 Energy flow in the plant.

consumption in the coils (ohmic loss), respectively. In an SCC device, P_{coil} is assumed as zero. On the other hand, f_{plant}, f_{aux}, and f_{CD} represent the ratio of the power for the

subsystems to the gross electricity, the efficiency of heating NB, and the efficiency of CD NB, respectively. The subsystem includes the coolant system, vacuum-pumping system, and the refrigerator system for cooling down the superconducting coils in an SCC device. The relations of these powers are shown below. We assumed that $f_{\rm plant}$ is 0.05 in both the SCC and NCC settings, as is the case of water cooling in reference [14], wherein 0.01 is for the primary-loop pumping power and 0.04 for the auxiliary functions. As the refrigerator power would be quite lower compared to $P_{\rm e-gross}$ in a device considered here with the major radius of ~3 m, the difference in $f_{\rm plant}$ between SCC and NCC settings is neglected.

$$P_{\rm e-net} = P_{\rm e-gross} - P_{\rm e-recirc}, \tag{10}$$

$$P_{\rm e-recirc} = \frac{P_{\rm CD}}{f_{\rm CD}} + \frac{P_{\rm aux}}{f_{\rm aux}} + f_{\rm plant}P_{\rm e-gross} + P_{\rm coil}. \tag{11}$$

2.5 Cost analysis

Because the primary objective of the device is to produce neutrons and not to generate electricity, the 'cost of neutron' (CON) was used for the evaluation of economy:

$$\text{CON} = \frac{\text{Annual cost [\$]} - \text{Annual income [\$]}}{\text{Annually neutron energy applied for FFR [kWh]}}. \tag{12}$$

Note that this is not the same as in our previous study [4], where the denominator was the total annual neutron energy. The denominator in Eq. (12) is smaller than the total annual neutron energy by a factor of $S_{\rm FFR}/S_{\rm FW}$.

The income by selling electricity at the market price is subtracted from the total cost to evaluate the net cost. The market price was determined by consumer price index (CPI) and the exchange rate. First, we referred to the annually averaged market price of power selling, 9.87 2013 ¥/kWh, of a Japanese power company in the 2013 fiscal year. We converted the unit of yen to the unit of the dollar using the exchange rate, 100.35 ¥/$, in the same year. Finally, we converted the unit of 2013 $/kWh to 2003 $/kWh, which is the unit of CON, using the 2003 CPI, 183.96, and the 2013 CPI, 232.96. Thus, we estimated the unit price of power selling at 77.7 2003 mill/kWh (1 mill is 0.001 $).

Annual cost is composed of total capital cost, operation and maintenance cost, replacement cost, fuel cost, and decomposition cost. Evaluation of these costs is based on the existing engineering and cost models in PEC. The mostly used cost evaluation is referred to [14], but we used the cost of the primary loop with Li coolant in [14] as the cost of the primary loop with Na coolant assumed in this study, as in SABR. The cost of primary loop was approximately 6.5% of the total capital cost. Here, we considered the fact that Na is cheaper than Li. We also assumed the operation period to be 30 years, plant availability ($f_{\rm avail}$) of NCC settings at 75%, which is the same value for ARIES–ST [6], and SCC settings at 60% of the standard values, which comes from the report that SABR can burn the TRU discharged annually from three 1000-MW (electric) fission plants if $f_{\rm avail}$ of SABR is 60% [3], and is scanned around it.

3. Scan in NCC Settings

The plasma and engineering parameters and economy have been evaluated by PEC in the range between A = 1.625 and 3 for NCC settings, at intervals of 0.125. The plasma size (major radius, minor radius, and elongation) is determined for each aspect ratio to satisfy the fixed area of FFR. We scanned some parameters, beginning with A.

3.1 A dependence in NCC settings

We scanned A in NCC settings, with the standard $t_{\rm sh}$ of 0.26 m. The results of CON, CON_capital, and CON_income are shown in Fig. 7. Here, the CON_capital and CON_income are defined by Eqs. (13) and (14).

$$\text{CON\_capital} = \frac{\text{Annual capital cost [\$]}}{\text{Annually neutron energy applied for FFR [kWh]}}, \tag{13}$$

$$\text{CON\_income} = \frac{\text{Annual income [\$]}}{\text{Annually neutron energy applied for FFR [kWh]}}. \tag{14}$$

We could observe that CON_income increases with A for nearly $A \leq 2.125$, then it decreases approximately at $A > 2.125$. On the other hand, the CON_capital increases with A constantly. The CON has the minimum at roughly $A = 2.0$. The economical optimal condition is

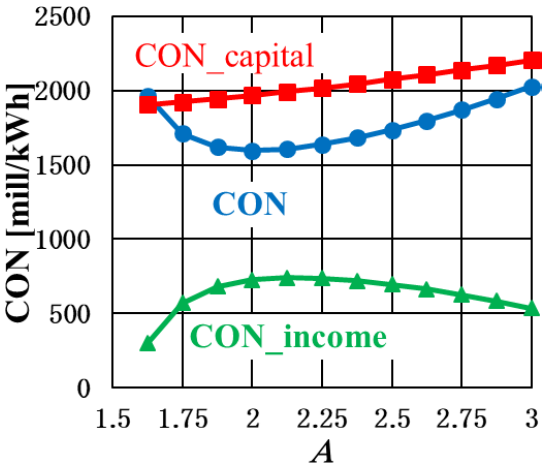

Fig. 7 CON, CON_capital, and CON_income as functions of A in NCC settings, with the standard $t_{\rm sh}$. At approximately A = 2.0, the value of CON becomes the minimum.

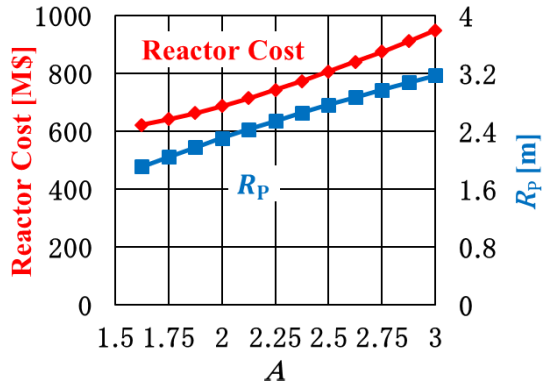

Fig. 8 Reactor cost and R_P as functions of A in NCC settings, with the standard t_{sh}. R_P is a measure of the reactor size, so that reactor cost increases with R_P.

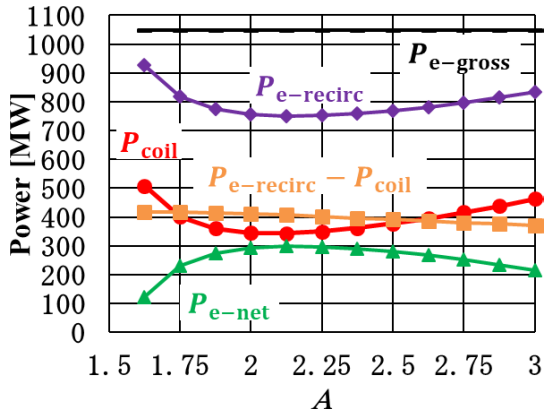

Fig. 9 $P_{e-gross}$, $P_{e-recirc}$, P_{coil}, $P_{e-recirc} - P_{coil}$, and P_{e-net} as functions of A in NCC settings, with the standard t_{sh}. The dependence of P_{coil} on A is a dominant factor in determining those of $P_{e-recirc}$ and P_{e-net}.

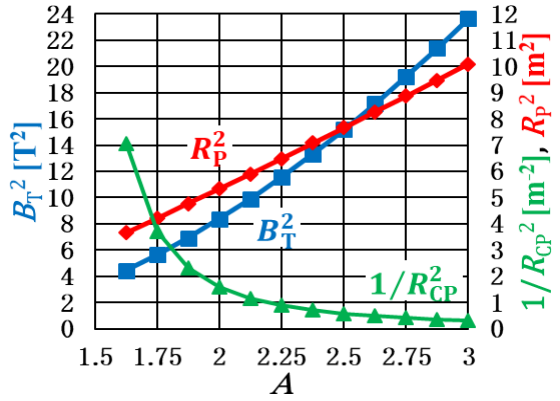

Fig. 10 R_P^2, B_T^2, and $1/R_{CP}^2$ as functions of A in NCC settings. $1/R_{CP}^2$ increases sharply with the decrease in A for $A \leq 2.0$ because of small space for CP; it decreases gradually with A for $A > 2.0$; R_P^2 and B_T^2 increase constantly with A.

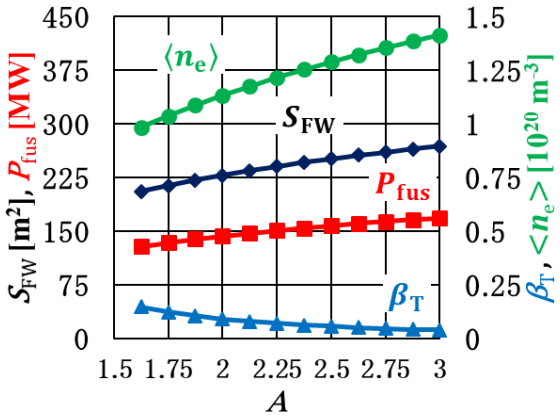

Fig. 11 P_{fus}, S_{FW}, $\langle n_e \rangle$, and β_T as functions of A in NCC settings.

located around this point.

The results of the reactor cost and R_P are shown in Fig. 8. Here, the reactor cost and R_P increases with A. R_P is a measure of the reactor size, so that the reactor cost increases with R_P.

The results of $P_{e-gross}$, $P_{e-recirc}$, P_{coil}, $P_{e-recirc} - P_{coil}$, and P_{e-net} are shown in Fig. 9. We fixed $P_{e-gross}$ to 1049 MW (electric). $P_{e-recirc}$ decreases with A for $A \leq 2.125$, then increases for $A > 2.125$. Hence, P_{e-net}, the difference between $P_{e-gross}$ and $P_{e-recirc}$, also increases with A for $A \leq 2.125$, then decreases for $A > 2.125$. P_{coil} has similar dependence on A, to that of $P_{e-recirc}$. $P_{e-recirc}$ and P_{coil} have a minimum at approximately $A = 2.125$. The dependence of $P_{e-recirc} - P_{coil}$ on A, which shows the circulating power, except P_{coil}, is weaker than that of P_{coil}. Thus, the dependence of P_{coil} on A is a dominant factor in determining those of $P_{e-recirc}$, P_{e-net}, and CON_income in the NCC device, as is discussed in the previous study [4].

The dependence of P_{coil} on A can be understood as follows. Because the resistivity of the coil is inversely proportional to its cross-sectional area S_{coil}, we have $P_{coil} \propto I_{coil}^2/S_{coil}$, where I_{coil} is the coil current. From Ampere's law, we have $I_{coil} \propto R_P B_T$. As shown in the NCC settings in Fig. 1 (a), S_{coil} can be regarded as the cross-sectional area of CP. As a result, we have $P_{coil} \propto R_P^2 B_T^2/R_{CP}^2$. The results of R_P^2, B_T^2, and $1/R_{CP}^2$ are plotted as functions of A in Fig. 10. Note that $1/R_{CP}^2$ increases sharply with the decrease in A for $A \leq 2.0$ due to the small space for CP, while it decreases gradually with A for $A > 2.0$. R_P^2 and B_T^2 increase with A constantly. As a result, P_{coil} has the minimum at roughly $A = 2.125$.

The results of P_{fus}, S_{FW}, $\langle n_e \rangle$, and β_T are shown in Fig. 11, where $\langle n_e \rangle$ and β_T are the average electron density and toroidal beta, respectively. We could see that S_{FW} increases with A, because of the dependence of R_P in A, as shown in Fig. 8. Moreover, P_{fus} increases with A in order to fix $P_{fus} S_{FFR}/S_{FW}$ as S_{FFR}/S_{FW} decreases with A; $\langle n_e \rangle$ also increases with A because of $P_{fus} \propto \langle n_e \rangle^2 \langle T_e \rangle^2$, where $\langle T_e \rangle$ is the average electron temperature and is fixed (Eq. (7) and Sec. 2.3); β_T decreases with A because of

$\beta_T = \beta_N I_P/(a_P B_T)$, where a_P is the plasma minor radius, β_N decreases with A as shown in Eq. (5) and Fig. 4, and $I_P/(a_P B_T)$ also decreases with A for a fixed safety factor. As a result, B_T^2 increases with increasing A because of $B_T^2 \propto \langle n_e \rangle/\beta_T$.

Consequently, CON_income decreases with the decrease in A for $A \leq 2.125$, because of increase in P_{coil} caused by the lack of CP space, while it decreases with A for $A > 2.125$, because of increase in I_{coil} caused by increasing required P_{fus} and decreasing β_T. As a result, CON_income has the maximum at approximately $A = 2.125$.

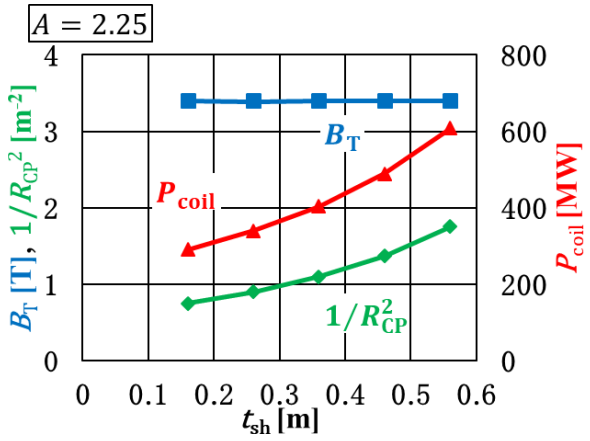

Fig. 12 Dependence of B_T, P_{coil}, and $1/R_{CP}^2$ on t_{sh}, at $A = 2.25$.

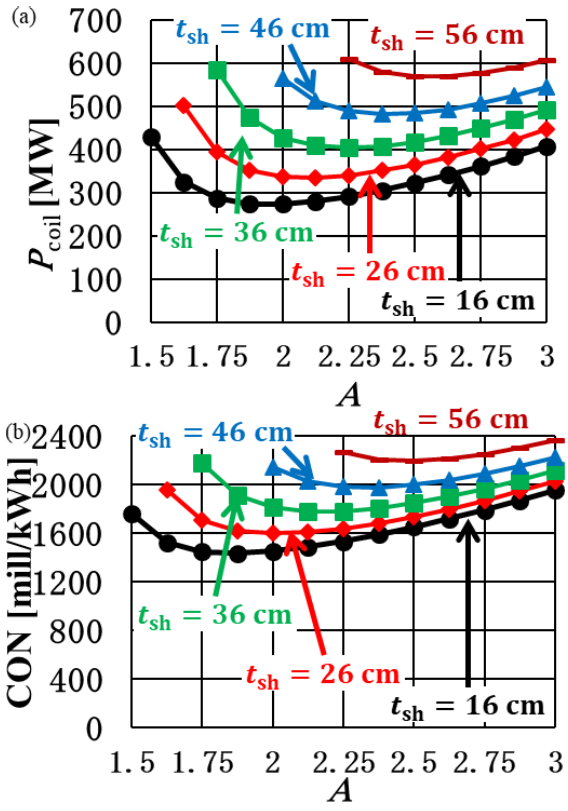

Fig. 13 Results of (a) P_{coil} and (b) CON of t_{sh} scanning.

3.2 Scanning t_{sh} in NCC settings

In the previous section, P_{coil} had a large impact on CON while the minimum P_{coil} was mainly determined by $1/R_{CP}^2$. As shown in Fig. 12, at fixed A and R_P, the CP radius, R_{CP}, becomes smaller as the thickness of the inboard shield (t_{sh}) becomes larger. Thus, $1/R_{CP}^2$ becomes larger, while B_T is independent of t_{sh} at a fixed A because P_{fus} and S_{FFR} are independent of t_{sh} at a fixed A. This will enhance the P_{coil} and the CON. In an NCC device, t_{sh} can be smaller than in an SCC device; nevertheless, if t_{sh} is not sufficient for an assumed operation duration, then CP will become brittle, and its conductivity will be lower due to the transmutation of Cu alloy [15]. The standard value 0.26 m for t_{sh} is assumed to be the value in the ARIES–ST design [7]. A transport analysis of neutrons and radiation which are necessary to determine the required minimal shield thickness is not done in this study yet. As shown in Eq. (1), R_{CP} depends on t_{sh}; therefore, we scanned t_{sh} in NCC settings.

The results of CON and P_{coil} are shown in Fig. 13. As t_{sh} increases, both become larger and have their minimum at a higher A. At $A = 2.25$, for instance, P_{coil} increases from 291 to 608 MW, while CON increases from 1519 to 2251 mill/kWh as t_{sh} increases from 16 to 56 cm. The optimum value of A for the minimum CON increased from 1.75 to 2.5 at this t_{sh} range.

4. Scan in SCC Settings and Comparison between NCC and SCC

4.1 A dependence in SCC settings

The A dependence of CON, CON_capital, and CON_income are shown in Fig. 14 for the standard f_{avail} of 60% in SCC settings.

At $A = 2.625$ and 3.625, the maximum toroidal field in the TF coil B_{max}, was higher than the critical magnetic field (11.8 T [10]); therefore, results are shown in the range $2.75 \leq A \leq 3.5$. We scanned A in this range at intervals of

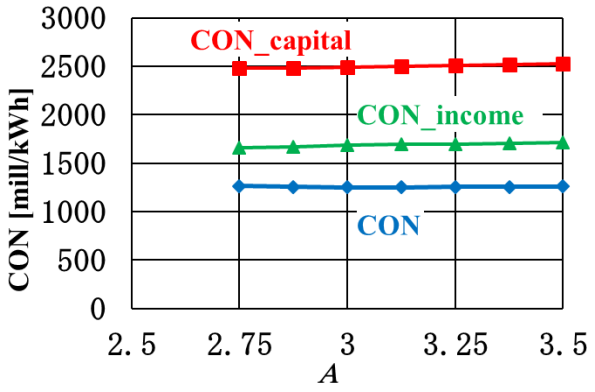

Fig. 14 CON, CON_capital, and CON_income as functions of A in SCC settings.

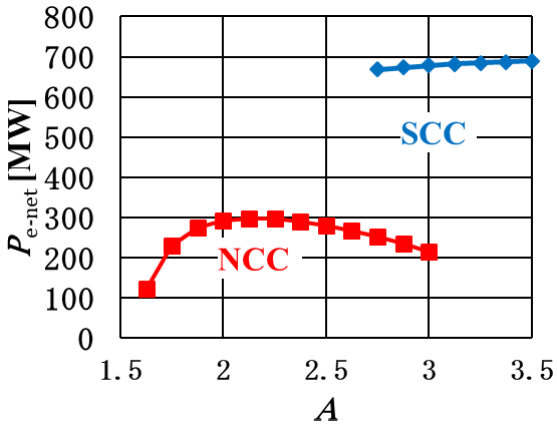

Fig. 15 Comparison of P_{e-net}. P_{e-net} of SCC settings is higher than that of NCC settings in the absence of P_{coil}.

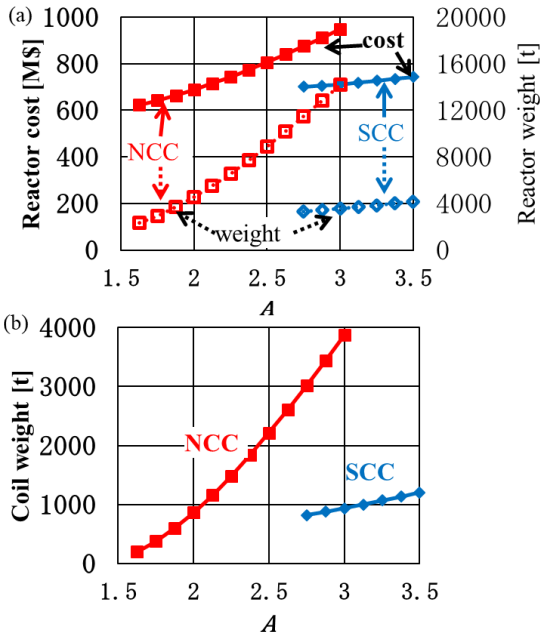

Fig. 16 Comparison of (a) reactor cost and reactor weight and (b) coils weight between the NCC settings and the SCC settings.

0.125. The high value of B_{max} was caused by the increase in B_{max}/B_T in a lower side of A while by the increase in B_T in a higher side of A [4].

As shown in Fig. 14, both the CON_income and CON_capital increase with A, with the latter increasing more rapidly than the former. The increment of CON_income for $A \leq 3.0$ is bigger than that for $A > 3.0$ because of the increasing q^* for $A > 3.0$ (described in Sec. 2.3, around Eq. (8)) causing decreasing I_P, deterioration of confinement of the plasma, and increasing power for heating the plasma. Consequently, the value of CON becomes minimum at approximately $A = 3.125$. The CON_income, however, increases with A constantly because the heating power $P_{aux} + P_{CD}$ is reduced due to enhance confinement with larger R_P.

Table 1 Formulas of weights of the TF coil.

SCC	TFC	$7.900\ [t/m^3] \times V_{TFC}\ [m^3]$
NCC	TFC	$2.295\ [t/m^3] \times V_{TFC}\ [m^3]$
	CP	$7.565\ [t/m^3] \times V_{CP}\ [m^3]$

4.2 Comparison between NCC settings and SCC settings

We compared the NCC settings of standard t_{sh}, with the SCC settings of standard f_{avail}. The comparison of P_{e-net} is shown in Fig. 15. As described before, in SCC settings, results are shown in a range of $2.75 \leq A \leq 3.5$. Thus, the P_{e-net} of SCC settings was higher than that of NCC settings in the absence of P_{coil}.

The reactor cost, the reactor weight, and the coil weight are compared in Fig. 16. We evaluated the weight of the TF coils by the formulas from Table 1. The dependence of the toroidal coil weight on A was relatively stronger in the NCC settings than in the SCC settings. We assumed that the outer TF coils were made from aluminum and referred to [6] for their weight density in NCC. Although the weight density of the TF coils was lower in NCC, their volume, V_{TFC}, was larger than in the SCC settings, due to the lower current density. The dependence of the reactor weight on A was far higher in the NCC settings than in the SCC settings due to the larger weight of the TF coils in the NCC settings. The CP was made as thicker as possible for lower ohmic loss; while in the case of SCC settings the thickness of its TF coils was determined by the fixed current density ($20.3\ MAm^{-2}$ [10]) and the required coil current, as described in Sec. 2.1. As a result, the dependence of the reactor weight and then the reactor cost of NCC settings on A was stronger than in the SCC settings. However, the dependence on A of the reactor cost was weaker than that of the reactor weight in both settings, because the reactor cost included the cost which does not depend on weight, for instance, cost of CD and heating systems that depend on the output power. The difference of the reactor cost at the optimal A between NCC ($A = 2.0$) and SCC ($A = 3.125$) settings was small.

4.3 Comparison between NCC and SCC settings with scanning f_{avail}

In-vessel components, such as shield, blanket, and divertor, must be operated by remote handling due to high radiation induced by DT fusion fast neutrons. One of the noteworthy differences between an NCC and an SCC fusion reactor is the difficulty in the maintenance of in-vessel components. In the NCC case, coils are demountable, as in CTF concepts [9], where the entire procedure of disassembly and assembly or vice-versa is estimated at

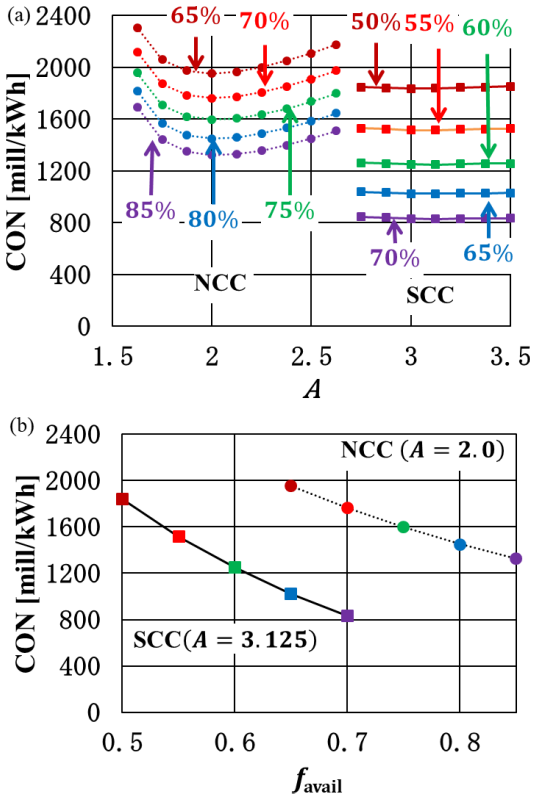

Fig. 17 (a) Comparison of CON between NCC and SCC settings with f_{avail} scanning. (b) Dependence of CON on f_{avail} at A, which has the minimum CON of each of NCC and SCC.

60 - 90 days, given adequate terms and conditions [9]. I.N. Sviatoslavsky et al. reported that replacement of the upper and lower diverters and CP would take approximately 1700 hours [16]. E.T. Cheng et al. reported that the replacement of the divertor plates and CP took more or less, 598 hours [17]. In the SCC case, because no demountability is available, we have to access to in-vessel components through the spaces between TFCs. In ITER, the maximum duration of the replacement was estimated at 9 months [18]. In JET, over 450 individual components were remotely handled within the JET torus during a 15-week period operating at 6 days per week, 20 hours daily [19].

Although there were plenty of reports regarding maintenance, we were not able to determine the appropriate f_{avail}; our f_{avail} of the standard value (75% for NCC and 60% for SCC) was an assumption. Therefore, we scanned the f_{avail} for both settings.

As shown in Fig. 17 (a), the CON of both of NCC and SCC decreases with increasing f_{avail}, while its dependence on A is weaker in the SCC settings because of the weaker A dependence of the capital cost and P_{e-net} in the SCC settings. In Fig. 17 (b), if the reduction of the f_{avail} of SCC as compared with NCC is 0.20–0.25, then the SCC settings have a higher economic potential than the NCC settings.

Table 2 shows the main parameters in the NCC and

Table 2 Main parameters near economical optimal A.

Parameter	NCC	SCC
Aspect ratio	2.00	3.13
Major radius [m]	2. 31	3.27
Minor radius [m]	1.15	1.05
Elongation	2.03	1.78
Triangularity	0.50	0.50
Plasma current [MA]	8.58	7.11
Bootstrap current fraction	0.57	0.56
Normalized beta	3.54	2.79
Toroidal beta [%]	9.10	3.72
Poloidal beta	0.89	1.09
q_{95}	3.76	3.00
Electron temperature (center/average) [keV]	15.0/ 7.50	15.0/ 7.50
Electron density $[10^{20}\mathrm{m}^{-3}]$ (center/ line average)	1.42/ 1.24	1.80/ 1.57
Greenwald fraction	0.60	0.76
H factor (98y2)	1.0	1.0
Fusion power [MW]	143.2	170.8
Average neutron wall load $[\mathrm{MW/m^2}]$	0.60	0.60
CD NB power [MW]	48.0	73.1
Heating NB power [MW]	131.2	84.1
Gloss electric power [MW]	1049.0	1049.0
Net electric power [MW]	293.1	682.1

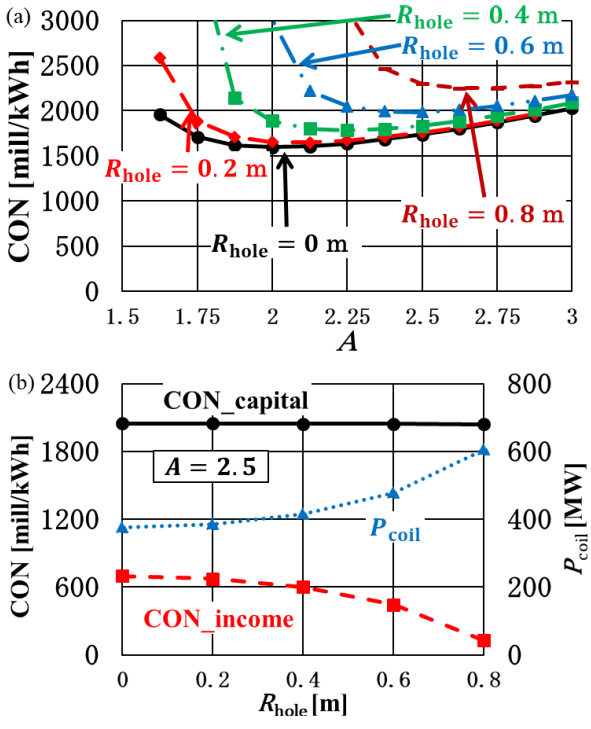

Fig. 18 (a) Results of CON with different R_{hole}. (b) Dependence of P_{coil}, CON_income, and CON_capital at A = 2.5 on R_{hole}.

SCC settings, with standard values, near the economically optimal A.

We assumed that all the available space within the inner shield was used for the CP in the NCC settings. As shown in Fig. 16, TF coil weight accounts for a large fraction of the reactor weight in the NCC settings. We checked if CON could be lowered by assuming a smaller cross-sectional area of CP with a central hole to reduce the weight of CP in NCC settings. The results are shown in Fig. 18 (a). The CON does not decrease but increases with increased CP hole radius $R_{\rm hole}$. It decreases the capital cost due to lower CP weight while the $P_{\rm coil}$ is increased due to higher current density in CP. The decrease in the total capital cost by the decrease in the CP volume is too small compared with the total cost, so that the decrease in the CON_capital is lower than the decrease in the CON_income, as shown in Fig. 18 (b). Therefore, we could not reduce the CON in the NCC settings by reducing the cross-sectional area of CP.

5. Summary and Discussions

We studied the economy of fusion neutron sources with the normal conductive coils (NCC) and super conducting coils (SCC) for transmutation of TRU by using a system code, PEC. We referred to SABR [3] for conditions of the blanket, which contains the transuranics and the thermal conditions. We assumed the plasma aspect ratio (A) dependencies of the plasma elongation (κ) [11], and A, the κ dependencies of normalized plasma beta ($\beta_{\rm N}$) [12], and power selling by net electricity [4].

The cost of neutron (CON) is used for evaluating the economy of the device. In the NCC settings, ohmic loss in the coils ($P_{\rm coil}$) was the dominant factor for economy in the low range of A due to a decrease in the income by power selling, as shown in the previous study [4]. It was caused by space reduction in the inboard toroidal coils (Center Post: CP). On the other hand, the increase in the capital cost due to the increase in reactor size was the dominant factor for the economy in the higher range of A. Consequently, in the NCC settings, CON became optimal at approximately $A = 2.0$. $P_{\rm coil}$ increased with increasing inboard shield thickness, $t_{\rm sh}$, due to the reduced space for CP. Larger $t_{\rm sh}$ resulted in CON degradation and shift of the economically optimal A to a higher value.

In the SCC settings, the variation of CON with A was relatively small compared with that of the NCC settings, mainly due to the absence of $P_{\rm coil}$ and fixed current density in the SCC. The increment of the capital cost with A was lower in the SCC settings than in the NCC settings, due to the smaller weight of coils with higher current density.

The dependence of reactor weight and reactor cost on A was stronger in the NCC settings than in the SCC settings due to the difference in each concept of coil design. NCC settings have $P_{\rm coil}$, so that the dependence of net electricity on A was stronger, while a larger net electricity was expected in SCC. We also found that when SCC settings have the sufficient plant availability, their economic potential was relatively higher. It should be noted that development of a complicated and reliable remote-handling system would be needed to achieve enough plant availability in an SCC device.

The present results might depend on the assumptions made for the analysis, including fixed conditions of reactor components like blankets, and first walls omission of the central solenoid and non-inductive CD. The area and thickness of the outer blanket and $t_{\rm sh}$ will be assessed by neutron and radiation transport analysis in the future. The possibility of inserting a central solenoid for plasma start-up will also be considered. The scenario of plasma start-up will be assessed by analysis of the CD.

Acknowledgments

The authors thank the reviewer for pointing out the conditions required to achieve the performance on transmutation of TRUs and the fission power, which was newly included in Sec. 2.2 in revising the manuscript.

[1] Z. Chen *et al*., Ann. Nucl. Energy **75**, 723 (2015).
[2] M. Kotschenreuther *et al*., Fusion Eng. Des. **84**, 83 (2009).
[3] W.M. Stacey *et al*., Nucl. Technol. **162**, 53 (2008).
[4] T. Fujita *et al*., Nucl. Fusion **57**, 056019 (2017).
[5] M.A. Abdou, Fusion Eng. Des. **27**, 111 (1995).
[6] R.L. Miller *et al*., Fusion Eng. Des. **65**, 199 (2003).
[7] M.S. Tillac *et al*., Fusion Eng. Des. **65**, 215 (2003).
[8] K. Yamazaki *et al*., Fusion Eng. Des. **81**, 1145 (2006).
[9] Y-K.M. Peng *et al*., Plasma Phys. Control. Fusion **47**, B263 (2005).
[10] S. Imagawa *et al*., J. Plasma Fusion Res. **11**, S1050 (2016).
[11] J.P. Lee *et al*., J. Plasma Phys. **81**, 515810608 (2015).
[12] C.P.C. Wong *et al*., Nucl. Fusion **42**, 547 (2002).
[13] J. Menard *et al*., Proc. 24th IAEA Fusion Energy Conf. FTP/3-4 (2013). (http://www-naweb.iaea.org/napc/physics/FEC/FEC2012/papers/379_FTP34.pdf)
[14] R.L. Miller, *et al*., UCSD-ENG-004, UCSD (1997).
[15] L.A. El-Guebaly *et al*., Fusion Eng. Des. **65**, 263 (2003).
[16] I.N. Sviatoslavsky *et al*., Fusion Eng. Des. **45**, 281 (1999).
[17] E.T. Cheng *et al*., Fusion Eng. Des. **38**, 219 (1998).
[18] R. Hannge *et al*., Nucl. Fusion **39**, 2043 (1999).
[19] A.C. Rolfe, Nucl. Energy **38**, 277 (1999).